

Article

# Capacitive Tuning of High Selective T-Shaped Band-Stop Filter: Theory and Experiment

Amit K. Sahu<sup>1</sup> , Dhruva C. Panda<sup>2</sup> , Rajeev K. Parida<sup>2</sup> 

<sup>1</sup>NMREC Autonomous Institute, Hyderabad, Telangana, 500088, [amitsku@gmail.com](mailto:amitsku@gmail.com),

<sup>2</sup>Berhampur University, Berhampur, Odisha 760007, [dcpanda@gmail.com](mailto:dcpanda@gmail.com)

**Abstract**— This paper develops an easy design analysis for a simple high selective T-shaped band-stop filter (BSF) loaded with a capacitance. It applies the developed design theory to obtain an appropriate capacitance value for tuning the cut-off frequency. This paper clearly explains the design mechanism for such a simple tunable BSF using ABCD matrices. Simulated filters loaded with capacitances (up to 1.1 pF) show a change in rejection frequencies from 2 GHz (un-tuned) down to 1.047 GHz with 50dB rejection and around 36% -3dB fractional bandwidth. It also shows the effect on pass frequencies which change from 1 GHz down to 111 MHz, while the separation between pass and stop frequency remains around 1 GHz. Measurements on fabricated prototypes match the simulation and theory for tunable frequencies closely. It also compares the performance of the filter with previously reported similar structures.

**Index Terms**— Band-stop filter, capacitive loading, T-shaped transmission line, tunable.

## I. INTRODUCTION

Band-stop filter (BSF) is an essential wireless component in both military and civilian applications. So, it continues to be an area of research interest within the realm of Radio Frequency (RF) and Microwave Technology. It is known that an appropriately designed T-shaped transmission line (TL) can act as a simple BSF. Its operating principle lies in the fact that, with an appropriate choice of length, the open-ended stub acts as a short at the cut-off frequency [1]. A tunable BSF provides many advantages like tunability, compactness, selectivity, cost-effectiveness, and spectrum management in RF and microwave circuits [2], [3]. Stop-band tunability over small ranges includes varactor [4], substrate integrated waveguide (SIW) resonator coupled microstrip line [5], and half mode SIW for flexibly controlled cut-off [6], [7]. A T-shaped TL BSF design makes frequency adjustment possible by inserting an inductive diaphragm at the stub attachment point [8]. Integrating graphene oxide with T-shaped TL BSF results in switching between two frequencies, corresponding to the high and low states of the graphene oxide memristor [9]. Monolithic microwave integrated circuit (MMIC)-based quasi-absorptive bandstop filters (ABSFs) provide high rejection tunable BSF with low tuning range [10], but the structures are complex. However, for frequency tuning, a varactor is common [2], [10]-

[14] in planar circuits.

Open literature lack the theory of how the capacitor affects frequency tuning, although the principle is available. There are no general design equations for tunable T-shaped TL BSF. When there any design equation exists, it is only for special cases. So, the design is mostly dependent on electromagnetic (EM) simulation. As the simulation requires many cycles of iterations, it is computation-intensive and time-consuming. Thus, it is important to focus on developing a design theory that shall require fewer EM simulation cycles and hence consume less computational time.

As discussed, existing works do not report any analytical method for designing tunable T-shaped TL BSF. The novelty of this paper lies in developing simple general design equations for generating the parameters of the capacitively-loaded T-shaped TL BSF using transmission-line model calculations based on ABCD matrices. Finally, EM simulations using Ansys HFSS and measurements on prototype models verify the theory.

## II. CAPACITIVELY LOADED BSF DESIGN

The ABCD matrix of a T-shaped planar TL (Fig. 1(A)) is  $M_T = M_1 M_2 M_1$ .  $M_1$  and  $M_2$  are the ABCD matrices of arm#1 of length  $l_1$  (and arm#2 of length  $l_1$ ), and the loaded stub of length  $l_2$ , respectively.

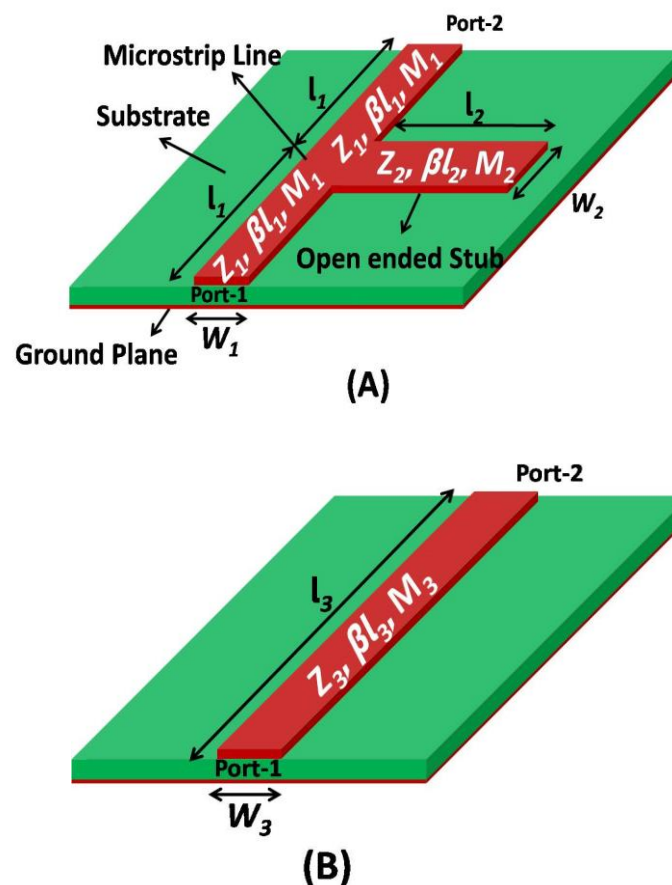


Fig. 1. T-shaped open stub filter and its equivalent microstrip TL.

$$M_1 = \begin{bmatrix} \cos \beta l_1 & jZ_1 \sin \beta l_1 \\ jY_1 \sin \beta l_1 & \cos \beta l_1 \end{bmatrix} \quad (1)$$

$$M_2 = \begin{bmatrix} 0 & 1 \\ Y_{in} & 0 \end{bmatrix} \quad (2)$$

$Y_{in}$  is the input admittance, looking into the capacitively-loaded stub, with loading capacitance  $C$ , from the main signal line, expressed as:

$$Y_{in} = Y_2(j\omega C + jY_2 \tan \beta l_2) / (Y_2 - \omega C \tan \beta l_2) \quad (3)$$

Thus, 
$$M_T = \begin{bmatrix} M_{T(1,1)} & M_{T(1,2)} \\ M_{T(2,1)} & M_{T(2,2)} \end{bmatrix}$$

with 
$$M_{T(1,1)} = \cos 2\beta l_1 + jY_{in}Z_1 \sin \beta l_1 \cos \beta l_1 \quad (4a)$$

$$M_{T(1,2)} = 2jZ_1 \sin \beta l_1 \cos \beta l_1 - Y_{in}Z_1^2 \sin^2 \beta l_1 \quad (4b)$$

$$M_{T(2,1)} = 2Y_1 \sin \beta l_1 \cos \beta l_1 + Y_{in} \cos^2 \beta l_1 \quad (4c)$$

$$M_{T(2,2)} = jZ_1Y_{in} \sin \beta l_1 \cos \beta l_1 + \cos 2\beta l_1 \quad (4d)$$

Considering a section of TL as equivalent (Fig. 1(B)) to this T-shaped filter [15] and equating their ABCD matrices, results in:

$$M_3 = \begin{bmatrix} \cos \beta l_3 & jZ_3 \sin \beta l_3 \\ jY_3 \sin \beta l_3 & \cos \beta l_3 \end{bmatrix} = M_T \quad (5)$$

At the angular pass frequency  $\omega_p$  (with phase constant  $\beta_p$ ), equating corresponding elements of matrices  $M_3$  and  $M_T$  gives

$$Y_1 = Y_3 \left( \frac{\tan \beta_p l_1 (1 + \cos \beta_p l_3)}{\sin \beta_p l_3} \right) \quad (6)$$

$$Y_{in} = \frac{jY_3 \sin \beta_p l_3 (\cos \beta_p l_3 - \cos 2\beta_p l_1)}{\cos^2 \beta_p l_1 (\cos \beta_p l_3 - 1)} \quad (7)$$

Using  $Y_{in}$  from equation (3) in equation (7) results in:

$$Y_2 = \frac{-B \pm \sqrt{B^2 - 4AD}}{2A} \quad (8)$$

$$A = \tan \beta_p l_2 \cos^2 \beta_p l_1 - \tan \beta_p l_2 \cos^2 \beta_p l_1 \cos \beta_p l_3$$

$$B = \omega C \cos^2 \beta_p l_1 + Y_3 \sin \beta_p l_3 \cos \beta_p l_3 - \omega C \cos^2 \beta_p l_1 \cos \beta_p l_3 - Y_3 \sin \beta_p l_3 \cos 2\beta_p l_1$$

$$D = \omega C Y_3 \sin \beta_p l_3 \tan \beta_p l_2 \cos 2\beta_p l_1 - Y_3 \omega C \tan \beta_p l_2 \sin \beta_p l_3 \cos \beta_p l_3$$

A judicious choice of the equivalent TL section is important for the design as it can simplify the above equations. An electrical length (i.e.  $\beta_p l_3$ ) of 90 degree simplifies these equations to

$$Y_1 = Y_3 \tan \beta_p l_1 \quad (9)$$

$$Y_{in} = \frac{jY_3 \cos 2\beta_p l_1}{\cos^2 \beta_p l_1} \quad (10)$$

$$A = \tan \beta_p l_2 \cos^2 \beta_p l_1$$

$$B = \omega C \cos^2 \beta_p l_1 - Y_3 \cos 2\beta_p l_1$$

$$D = \omega C Y_3 \tan \beta_p l_2 \cos 2\beta_p l_1$$

These equations show that only the characteristic admittance of the stub line ( $Y_2$ ) depends on the loading capacitance  $C$ . For ease of changing the capacitance, it is desirable to start with a zero capacitance which is equivalent to an open-ended stub. So, for initial design  $C = 0$  is a desirable choice which simplifies the expression  $Y_2$  as:

$$Y_2 = Y_3 \left[ \frac{\cos 2\beta_p l_1}{\cos^2 \beta_p l_1 \tan \beta_p l_2} \right] \quad (11)$$

Equations (9) and (11) are sufficient for the initial design. However, they do not address the issue of selectivity.

A condition for good selectivity is  $\frac{Y_1}{Y_2} \geq 1$  [8]. Using this condition in the equations (9) and (11)

results in the inequality:

$$\frac{\tan 2\beta_p l_1 \tan \beta_p l_2}{2} \geq r_n \quad (12)$$

$r_n$  being the ratio of the two admittances. Thus, for a given length  $l_2$ , equation (12) fixes the lower

limit on the length  $l_1$  as:

$$l_1 \geq \frac{\tan^{-1}\left(\frac{2r_n}{\tan \beta_p l_2}\right)}{2\beta_p} \quad (13)$$

Similarly, equation (11) indicates the limit on  $\beta_p l_1$  to be  $\pi/4$ .

Therefore,

$$\frac{\tan^{-1}\left(\frac{2r_n}{\tan \beta_p l_2}\right)}{2\beta_p} \leq l_1 \leq \frac{\pi}{4\beta_p}$$

At the cut-off frequency, the stub must act as a short. As quarter wave open stub behaves like a short, so for a sharp cut-off,  $\beta_p l_2$  ( $\beta_c$  being phase constant at cut-off frequency) should be  $\pi/2$ . If the ratio between cut-off and pass frequency is  $r$ , then  $\beta_p l_2$  is  $\pi/2r$ .

#### A. Algorithm for initial design

The calculations of the dimensions in the design follow an algorithm, the steps of which are presented below. Different parameters used in the algorithm are:  $W_{min}$  - the smallest width that can be fabricated in the laboratory;  $\omega_p$  - angular pass frequency;  $c$  - speed of light in free space;  $\omega_c$  - angular cut-off frequency;  $\epsilon_r$  - substrate relative permittivity;  $Z_3$  - characteristic impedance of imaginary transmission line;  $r$  - the ratio of cut-off to pass frequency;  $r_n$  - the ratio of stub to main line characteristic impedances.

BEGIN

Step 1: Initialize the parameters  $W_{min}, \omega_p, r, \epsilon_r, Z_3 = 50\Omega$

Step 2: Calculate  $\omega_c \leftarrow r\omega_p; v \leftarrow \frac{c}{\sqrt{\epsilon_r}}; \beta_p \leftarrow \frac{\omega_p}{v}; \beta_c \omega_c \leftarrow \frac{\beta_c \omega_c}{v}$

Step 3: Calculate  $l_3 \leftarrow \frac{\pi}{2\beta_p}, l_2 \leftarrow \frac{\pi}{2r\beta_p}$

Step 4a: Set  $r_n > 1$

Step 4b: Set  $l_1 \leftarrow \frac{\tan^{-1}\left(\frac{2r_n}{\tan \beta_p l_2}\right)}{2\beta_p}$

Step 5: If  $\beta_p l_1 \geq \frac{\pi}{4}$

then

choose new  $r_n$  and go to step 4b

else

go to step 6

Step 6: Calculate  $Y_1 \leftarrow Y_3 \tan \beta_p l_1$

Step 7: Calculate  $W$  for  $Y_1$

If  $W < W_{\min}$

then

select new  $r_n$  and go to step 4b

else

go to step 8

Step 8: Find  $Y_2 \leftarrow \frac{Y_1}{r_n}$

END

A capacitive loading of the shunt stub tunes the cut-off frequency of the initial T-shaped TL BSF design. At the tuned cut-off frequency, the capacitance loaded shunt stub must act as a short circuit. So the denominator of equation (3) should vanish at the cut-off frequency. Accordingly, the required capacitance for the desired cut-off frequency is

$$C = \left( \frac{Y_2}{\omega_c} \right) \cot \beta_c l_2 \quad (14)$$

The capacitance also affects the pass frequency ( $\omega_p$ ). The relationship between pass frequency and capacitance using equations (3) and (4a) is

$$\omega_p = \left( \frac{Y_2}{C} \right) \left( \frac{2Y_1 \cos 2\beta_p l_1 - Y_2 \tan \beta_p l_2 \sin 2\beta_p l_1}{2Y_1 \tan \beta_p l_2 \cos 2\beta_p l_1 + Y_2 \sin 2\beta_p l_1} \right) \quad (15)$$

Using the tuning capacitance obtained from equations (14) in (15) and applying simple numerical techniques, one can determine the pass frequency.

### III. RESULTS AND DISCUSSION

Here, a simple BSF design with  $f_c = 2$  GHz,  $r = 2$  ( $f_p = 1$  GHz) illustrates the application of the proposed design theory. As mentioned in the algorithm, the design assumes  $Z_3 = 50 \Omega$ . It also obtains  $l_3$  and  $l_2$  to be 35.75 mm and 17.79 mm, respectively. The next step is determination of  $r_n$ .

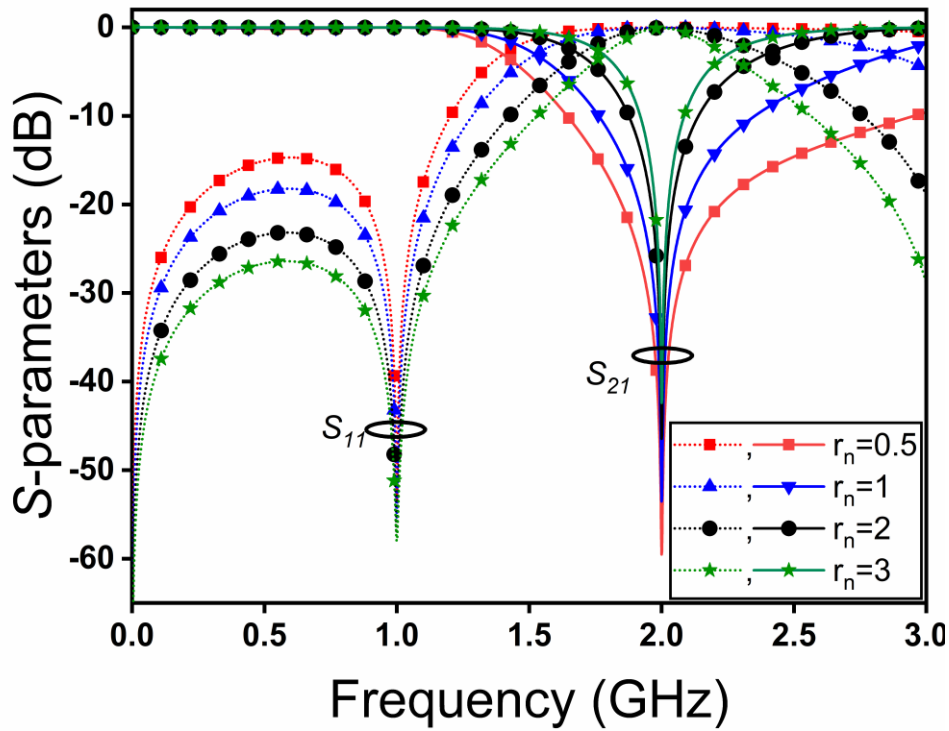


Fig. 2. Comparison of selectivity for different  $r_n$  values using HFSS

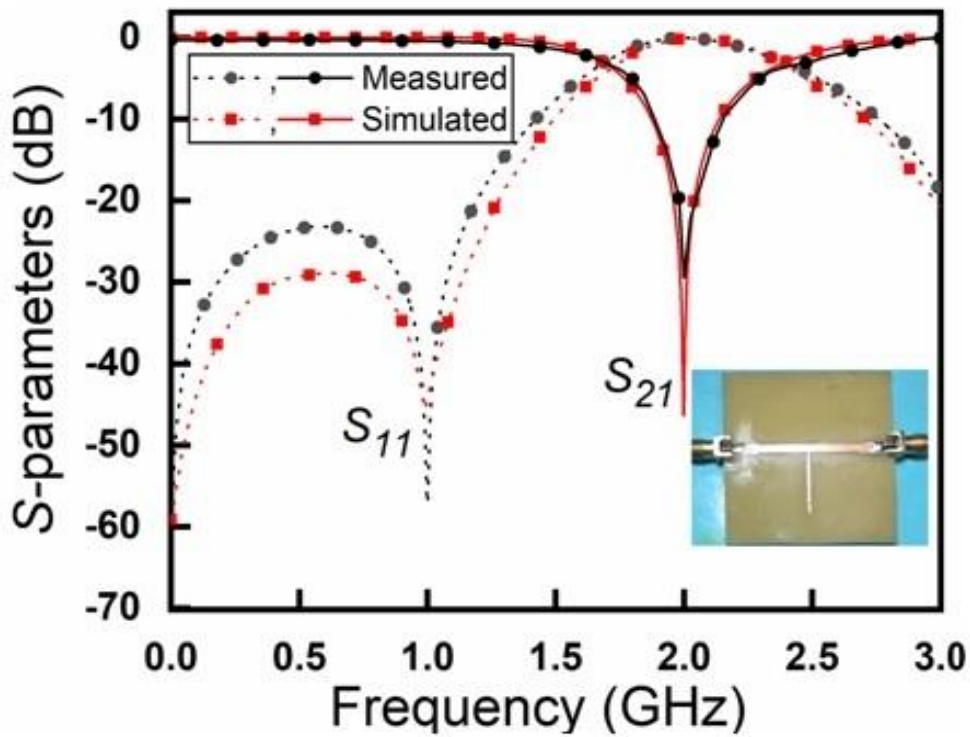


Fig. 3. Measured and simulated  $S$ -parameters of the BSF without tuning capacitance ( $C=0$ ; inset: Fabricated T shaped BSF prototype)

Figure 2 illustrates the selectivity for different  $r_n$  values. It is observed that  $r_n = 2$  yields good selectivity. Although selectivity improves further with increasing  $r_n$ , it becomes difficult to realize a

trace of smaller width to match the characteristic impedance of the TL section. Therefore,  $r_n = 2$  is a good choice for this design. Accordingly,  $l_1 = 15.1$  mm,  $Y_1 = 0.0156 \text{ } \Omega^{-1}$  ( $W_1 = 1.96$  mm), and  $Y_2 = 0.0078 \text{ } \Omega^{-1}$  ( $W_2 = 0.3$  mm) where  $W_1$  and  $W_2$  are widths of the respective TL sections. The resulting T-section prototype is fabricated using FR4 epoxy with a relative permittivity 4.4 and a loss tangent of 0.02, employing the wet etching technique.

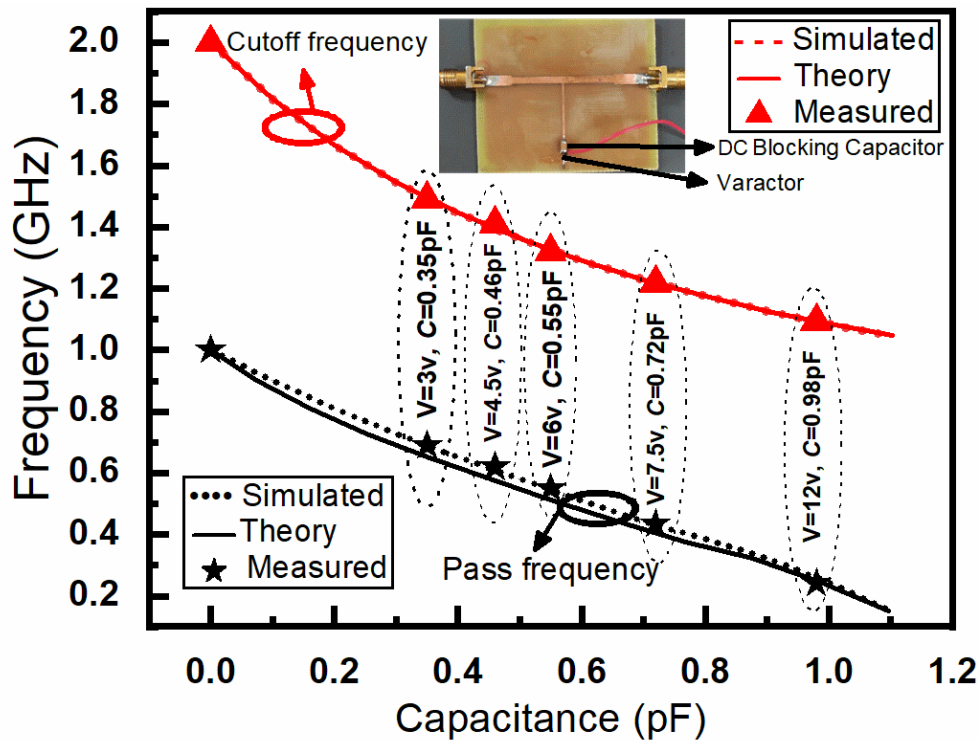


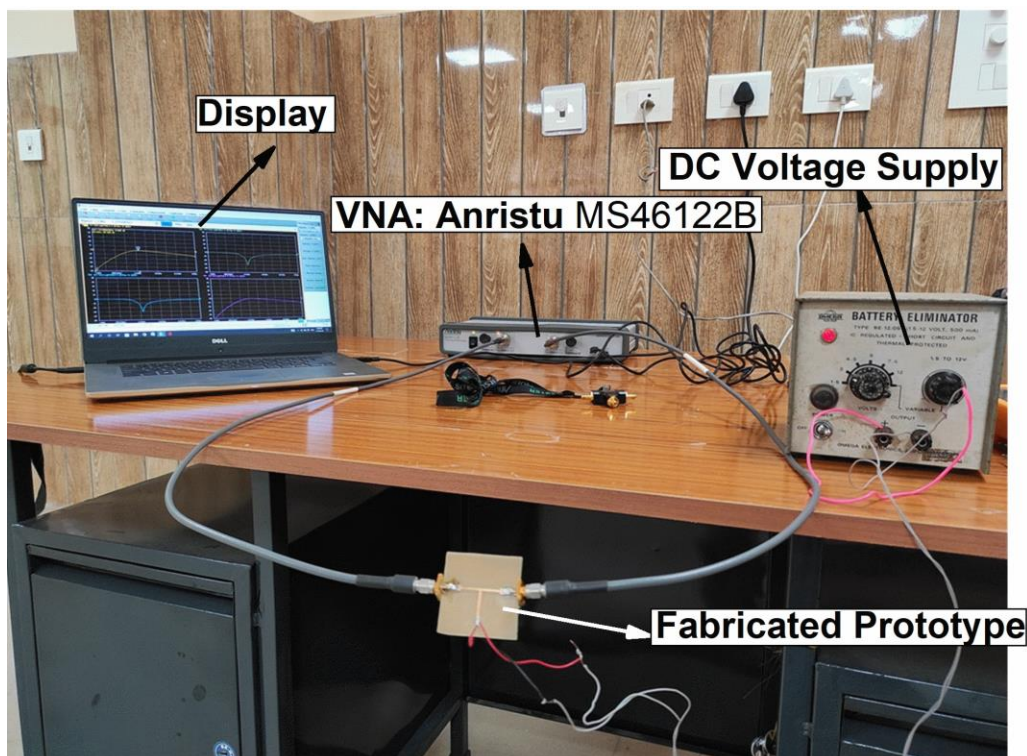
Fig. 4. Comparison of theoretical, simulated, and measured frequencies (cut-off and pass) for different values of capacitances (inset: Fabricated tunable BSF prototype)

Figure 3 compares simulated and measured results for a prototype fabricated filter (Fig. 3: inset). The center frequencies of the pass-band and stop-band correspond to dips in  $S_{11}$  and  $S_{21}$ . From the figure these two frequencies are around 1 GHz and 2 GHz, respectively. The measured result follows the simulated one closely.

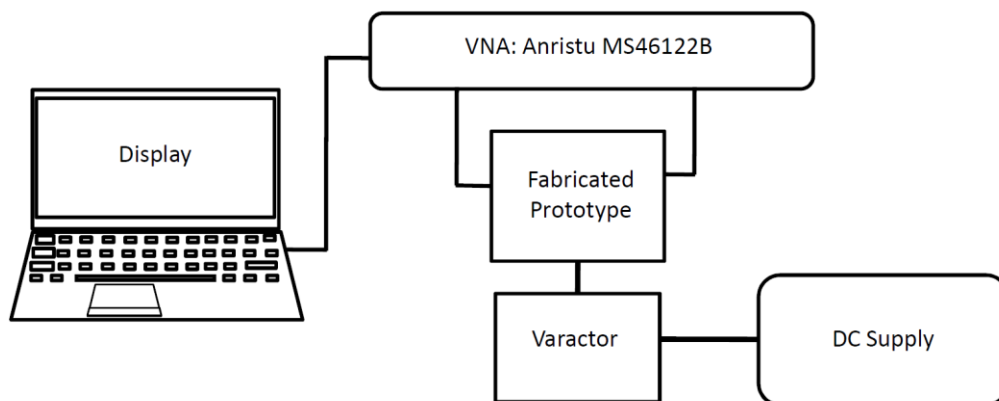
The plots in Fig. 4 show that as the capacitive load varies from 0 pF to 1.1 pF, the center frequencies of the stop-band and pass-band vary from 2 GHz to 1.047 GHz, and 1 GHz to 111 MHz, respectively. In addition to tuning, the stop-band rejection depth and the fractional bandwidth ( $= \frac{\Delta f}{f_c} \times 100\%$ , where,  $\Delta f$  is the difference between the band edges and  $f_c$  is the center frequency) of the filter are also obtained [4], [16]. This proposed filter exhibits 50dB rejection with around 36% -3dB

fractional bandwidth. The 30dB roll-off factor  $\left( \zeta = \frac{\alpha_{30dB} - \alpha_{3dB}}{f_{30dB} - f_{3dB}} \right)$  is found to be 190dB/GHz,

which justifies high selectivity [17]. Inset of Fig. 4 shows the prototype of a fabricated filter with varactor (SMV2019-79LF) loaded shunt stub. This inset shows the tuning arrangement using the varactor and DC blocking capacitor. Application of DC bias changes the capacitance of the varactor. Figure 4 shows the tuning of cut-off frequency with the change in capacitance. It also shows the effect of capacitance on pass frequency. The separation between cut-off and pass frequency remains almost constant with change in capacitance. The curves corresponding to measurement, theory, and simulation have good matching. Thus, the proposed theory is appropriate in terms of validation with EM simulation and measurement. The  $S$ -parameters of all prototypes are measured using the Anristu MS46122B VNA (Fig. 5(A)). Figure 5(B) represents the schematic diagram of the measurement setup.



(A)



(B)

Fig. 5. Measurement setup using ANRISTU MS46122B VNA

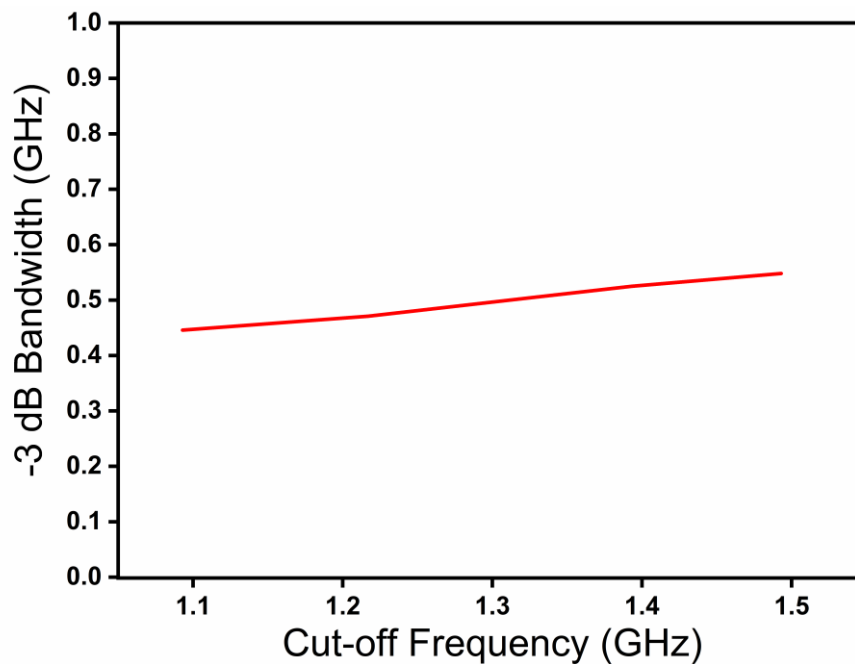


Fig. 6. -3dB bandwidth of the BSF for different tuning frequencies

TABLE I. PERFORMANCE COMPARISON TABLE

References	Tuning Mechanism	Rejection (dB)	Frequency Tuning Range (GHz)	Fractional Bandwidth % @ -3dB	Stop-Band Return Loss (dB)	Roll-off Factor $\zeta$
[4]	Varactor	27	0.66-0.99 (40%)	18	0.8	>195
[18]	Varactor	>40	2.22-3.13 (34%)	0.5	0	>45
[19]	Varactor	30	11.3-16.5 (37%)	14.36	1.5	>31.76
[5]	SIW	25	2.8-3.4 (19%)	> 3.1	1.5	>115
[20]	SIW	40	2.66-3.34 (23%)	0.035	0.79	>135
[9]	Graphene	28	2.308-3.143 (34%)	> 40	NA	>68
[10]	MMIC	>40	8.7-10.5 (19%)	> 7.73	NA	>45
[21]	Micromachine	>30	4-8 (67%)	> 6	> 1	>400
[22]	Substrate integrated Coaxial (SIC)	30	3.6-4.6 (24%)	>5.54	2	>150
This Work	Varactor	>50	1.047-2.00 (63%)	36±6	0.14	190

Figure 6 shows the effect of tuning cut-off frequency (2 GHz to 1.047 GHz) on -3dB bandwidth. The fractional bandwidth increases with increasing cut-off frequency. Table I compares the prototype with the state-of-art designs in the literature in terms of design metrics such as fractional bandwidth, tuning range, rejection, stop-band return loss, and selectivity. The table shows that the prototype has a broad tuning range, high selectivity, and high rejection depth compared to other reported BSFs. Moreover, it

has the simplest design compared to other such tunable BSFs.

#### IV. CONCLUSIONS

This work focused on designing a high selective tunable but simple BSF. It developed the appropriate theory for analyzing a capacitively-loaded T-shaped TL BSF. Then, it extended this theory to obtain design parameters like characteristic impedances and tuning capacitance for high selective BSF. It verified the developed theory with EM simulations and measurements on prototypes. Fabrication limitations at our laboratory restrict dimensions up to 1 decimal point in mm, requiring rounding up the calculated dimensions. In practice, it marginally affects the characteristic impedance and electrical length, which may be the reason for minor discrepancies between calculated, simulated and measured results. The developed theory can find applications in tunable BSF design using varactors and other loading elements.

#### ACKNOWLEDGMENT

Amit Kumar Sahu acknowledges the Council of Scientific and Industrial Research (CSIR), Govt. of India for providing fellowship (File No.: 09/297(0077)/2017-EMR-I, dated: 09/08/2018). We are thankful to Prof. R. K. Mishra, Berhampur University, for his valuable suggestions.

#### REFERENCES

- [1] A. Zahedi, F. A. Boroumand, and H. Aliakbrian, "Analytical transmission line model for complex dielectric constant measurement of thin substrates using T-resonator method," *IET Microwaves, Antennas & Propagation*, vol. 14, pp. 2027–2034, 2020.
- [2] A. Rajput and B. Mukherjee, "Electronically tunable UWB band stop filter using varactor diode," *AEU - International Journal of Electronics and Communications*, vol. 164, p. 154610, 2023.
- [3] K. D. Chavda and A. K. Sarvaiya, "Development of reconfigurable band stop filter using metamaterial for WLAN application," *2022 Photonics & Electromagnetics Research Symposium (PIERS)*, pp. 854–861, 2022.
- [4] A. Ebrahimi, T. Baum, J. Scott, and K. Ghorbani, "Continuously tunable dual-mode bandstop filter," *IEEE Microwave and Wireless Components Letters*, vol. 28, pp. 419–421, 2018.
- [5] S.W. Jeong and J. Lee, "Frequency- and bandwidth-tunable bandstop filter containing variable coupling between transmission line and resonator," *IEEE Transactions on Microwave Theory and Techniques*, vol. 66, pp. 943–953, 2018.
- [6] J. Hinojosa, M. Rossi, A. Saura-Ródenas, A. Álvarez-Melcón, and F. L. Martínez-Viviente, "Compact bandstop half-mode substrate integrated waveguide filter based on a broadside-coupled open split-ring resonator," *IEEE Transactions on Microwave Theory and Techniques*, vol. 66, pp. 3001–3010, 2018.
- [7] W. Xu *et al.*, "Tunable bandstop HMSIW filter with flexible center frequency and bandwidth using liquid crystal," *IEEE Access*, vol. 7, pp. 161308–161317, 2019.
- [8] Y. Kusama and R. Isozaki, "Compact and broadband microstrip band-stop filters with single rectangular stubs," *Applied Sciences*, vol. 9, 2019.
- [9] H. Abunahla, R. Gadhafi, B. Mohammad, A. Alazzam, M. Kebe, and M. Sanduleanu, "Integrated graphene oxide resistive element in tunable RF filters," *Scientific Reports*, vol. 10, p. 13128, 2020.
- [10] K. Zhao and D. Psychogiou, "X-band MMIC-based tunable quasi-absorptive bandstop filter," *IEEE Microwave and Wireless Technology Letters*, vol. 33, pp. 391–394, 2023.
- [11] C.-H. Ko, A. Tran, and G. M. Rebeiz, "Tunable 500–1200-MHz dual-band and wide bandwidth notch filters using RF transformers," *IEEE Transactions on Microwave Theory and Techniques*, vol. 63, pp. 1854–1862, 2015.
- [12] M. Fan, K. Song, Y. Zhu, and Y. Fan, "Compact bandpass-to-bandstop reconfigurable filter with wide tuning range," *IEEE Microwave and Wireless Components Letters*, vol. 29, pp. 198–200, 2019.
- [13] Y. I. A. Al-Yasir *et al.*, "A varactor-based very compact tunable filter with wide tuning range for 4G and sub-6 GHz 5G communications," *Sensors*, vol. 20, 2020.
- [14] Y. Wang, J. Chen, and K.-D. Xu, "A system of tunable bandstop filters with wide tuning range of 1-6-GHz," in *2019 International Workshop on Electromagnetics: Applications and Student Innovation Competition (iWEM)*, pp. 1–2, 2019.

- [15] W. H. Tu and K. Chang, "Compact second harmonic-suppressed bandstop and bandpass filters using open stubs," *IEEE Transactions on Microwave Theory and Techniques*, vol. 54, pp. 2497–2502, 2006.
- [16] J. S. Hong, and M. J. Lancaster, *Microstrip filters for RF/microwave applications*, John Wiley & Sons Ltd, pp. 29–76, 2001.
- [17] M. Hayati, S. Naderi, and F. Jafari, "Compact microstrip lowpass filter with sharp roll-off using radial resonator," *Electronics Letters*, vol. 50, pp. 761–762, 2014.
- [18] M. K. Mandal, J. Mandal, and M. Kahar, "Electronically tunable dual-band bandstop filter using a folded microstrip coupled-line," in *2018 IEEE MTT-S International Microwave and RF Conference (IMaRC)*, pp. 1–4, 2018.
- [19] Q. Li, X. Chen, P.-L. Chi, and T. Yang, "Tunable bandstop filter using distributed coupling microstrip resonators with capacitive terminal," *IEEE Microwave and Wireless Components Letters*, vol. 30, pp. 35–38, 2020.
- [20] S. Nam, B. Lee, and J. Lee, "Frequency-tunable substrate-integrated waveguide filter using contactless rotatable flaps," in *2019 IEEE MTT-S International Microwave Symposium (IMS)*, pp. 842–845, 2019.
- [21] Y. Feng, S. Tiwari, S. A. Bhave, and R. Wang, "Micromachined tunable magnetostatic forward volume wave bandstop filter," *IEEE Microwave and Wireless Technology Letters*, vol. 33, pp. 807–810, 2023.
- [22] D. Psychogiou, K. Zhao, and R. Gómez-García, "Dual-bandstop substrate-integrated-coaxial tunable and static RF filters," *IEEE Microwave and Wireless Components Letters*, vol. 31, pp. 1271–1274, 2021.